INVESTIGATION OF CHALCOGEN BIOISOSTERIC REPLACEMENT IN A SERIES OF HETEROCYCLIC INHIBITORS OF TRYPTOPHAN 2,3-DIOXYGENASE

Arina Kozlova[1,2,3], Léopold Thabault[1,4], Nicolas Dauguet[3], Marine Deskeuvre[1,4], Vincent Stroobant[2,3], Luc Pilotte[2,3], Maxime Liberelle[1], Benoît Van den Eynde[2,3,5], Raphaël Frédérick[1*].

[1] Louvain Drug Research Institute (LDRI), Université catholique de Louvain (UCLouvain), B-1200 Brussels, Belgium.

[2]Ludwig Institute for Cancer Research, Brussels B-1200, Belgium.

[3] de Duve Institute, UCLouvain, Brussels B-1200, Belgium.

[4] Pole of Pharmacology and Therapeutics, Institut de Recherche Expérimentale et Clinique (IREC), UCLouvain,B-1200 Brussels, Belgium.

[5] Walloon Excellence in Life Sciences and Biotechnology, Brussels B-1200, Belgium.

* Correspondence and Lead Contact: Raphaël Frédérick

Mailing address: LDRI, Avenue Mounier 73/B1.73.10, B-1200 Brussels, Belgium.

Phone number: +32 2 764 73 41

Email address: raphael.frederick@uclouvain.be

ABSTRACT

Selenium is an underexplored element that can be used for bioisosteric replacement of lower molecular weight chalcogens such as oxygen and sulfur. More studies regarding the impact of selenium substitution in different chemical scaffolds are needed to fully grasp this element's potential. Herein, we decided to evaluate the impact of selenium incorporation in a series of tryptophan 2,3-dioxygenase (TDO2) inhibitors, a target of interest in cancer immunotherapy. First, we synthesized the different chalcogen isosteres through Suzuki-Miyaura type coupling. Next, we evaluated the isosteres' affinity and selectivity for TDO2, as well as their lipophilicity, cellular toxicity on TDO2-expressing cell lines and microsomal stability. Overall, isosteric replacements did not disturb the on-target activity but allowed for a modulation of the compounds' lipophilicity, toxicity and stability profiles. The present work contributes to our understanding of oxygen/sulfur/selenium bioisosteric replacement towards

increasing structural options in medicinal chemistry for the development of novel and distinctive drug candidates.

Keywords: Isostery, chalcogen, selenium, atypical elements, tryptophan 2, 3-dioxygenase, cancer immunotherapy

Abbreviations:ROS, reactive oxygen species; TDO2, tryptophan 2, 3-dioxygenase; L-Trp, L-Tryptophan; TBAF, Tetra-n-ButylAmmonium Fluoride ; THF, tetrahydrofuran; ADME, Absorption, Distribution, Metabolism, and Excretion.

Graphical abstract:

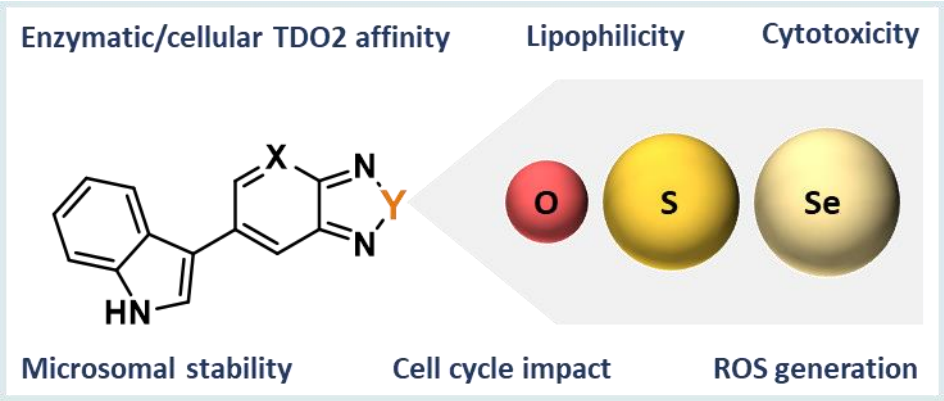

1. Introduction

Isosteric replacement is a commonly used strategy in rational drug design. This strategy assumes that functional groups with similar physicochemical properties can be interchanged to modulate efficacy, ADME/Tox, and off-target profiles.[1] Atoms from the chalcogen family, oxygen (O), sulfur (S) and selenium (Se), are a perfect example of this isosteric strategy. While O/S replacements are common in medicinal chemistry, integrating Se into drug-like structures only recently began to gain popularity and thus represents an underexplored research area.[2] The chalcogens share similar physicochemical properties and identical functional group types but present some notable differences. Indeed, the gradual increase in the atom size, particularly evident between O and S, results in lower electronegativity (respectively 3.44 and 2.58) and greater polarizability (**Figure 1**).[3] In turn, these

parameters lead to higher reactivity due to weaker bonding.[4] Moreover, the higher electronegativity of O allows it to be a great hydrogen bond acceptor. However, although they were long overlooked as hydrogen-bond acceptors, S and Se can also participate in hydrogen bonding interactions.[5,6] Finally, S and Se also have a more extensive range of oxidation states than O, allowing them to participate in various redox reactions.[7]

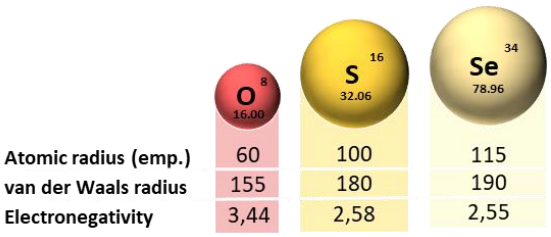

Figure 1. Comparison of oxygen, sulfur and selenium atoms. Radii are expressed in picometers. Atomic radii values are empirical, i.e. obtained from the distance between two atoms forming a bond in a crystal or molecule and is half of the value of the internuclear distance.[3,8] van der Waals radii are crystallographic radii.[9]

Se is a toxic yet essential trace element crucial for the regulation of cellular antioxidant systems.[10] It naturally occurs in the form of selenomethionine (Sem) or selenocysteine (Sec). The latter is present in the active sites of selenoproteins such as glutathione peroxidase (GPXs), thioredoxin reductase (TRXRs) and selenoprotein P (Sepp1).[11] Selenoproteins rely on dietary Se intake and a common set of cofactors for their synthesis.[12] Se deficiency is associated with numerous diseases and conditions, including neuromuscular and cardiovascular disorders, inflammation, neurodegeneration, endocrine disorders and higher cancer incidence and mortality rates.[12] It is thus not surprising that even despite the underwhelming outcomes of the Selenium and Vitamin E Cancer Prevention Trial (SELECT) a few years ago, many efforts aimed at designing and developing pharmaceutical agents that are Se-based or that target specific aspects of Se metabolism.[13,14] Today Se continues to draw interest in medicinal chemistry.[15]

The clinical drug Ebselen (2-phenyl-1,2-benzoselenazol-3-one, **Figure 2**), evaluated for different applications and diseases, is the most famous example of a Se-containing compound administered to humans. Ebselen catalyzes the reduction of hydroperoxides (ROS) in a glutathione-dependent manner

and can act as lithium mimetic.[16–18] While there were initial concerns regarding toxicity due to selenium liberation from Ebselen, it appears that there is no extrusion of the element from the heterocycle.[19] Multiple human clinical trials are currently ongoing, including one against SARS-CoV-2, as Ebselen inhibits its main protease.[20,21] An Ebselen analog, Ethaselen, an inhibitor of the mammalian thioredoxin reductase (TrxR), is currently evaluated in non-small cell lung carcinoma.[22] These examples demonstrated that a Se-containing drug is a realistic prospect, at least when the Se atom is in a cyclic moiety.

A few examples of bioisosteric replacement in the chalcogen series exist in the literature.[23–26] In 2011, Achilleon Pharmaceuticals replaced the thiophene group with selenophene in their type IIA Bacterial Topoisomerase inhibitors. The resulting compounds had similar on-target activity, a lower hERG channel inhibition and significant cytotoxicity or microsomal stability issues.[24] Other examples of chalcogen substitutions in non-cyclic moieties also led to non-toxic compounds.[25,26]

To our knowledge, there is no example of benzoxazole, benzothiadiazole and benzoselenodiazole replacement. The benzochalcogendiazole is a bicyclic scaffold consisting of an unsaturated 6-membered ring fused to a five-membered ring of two nitrogen atoms in positions 1, 3 and one chalcogen atom in between (**Figure 2**). It is a drug-like scaffold, present for instance, in the α2 adrenoceptor agonist drug tizanidine (Sirdalud®) and reported in the literature for various biological activities such as anti-proliferative and apoptogenic effects on tumor cells.[27,28] Moreover, 5-Bromobenzo[*c*][1,2,5]selenadiazole and Benzo[*c*][1,2,5]selenadiazole did not exhibit any cytotoxicity on various cancer cell lines, suggesting that this moiety might not present any intrinsic liabilities.[29] Finally, other Se-containing derivatives displayed free radical-scavenging activity.[30] Such antioxidant properties could be of interest in neurodegenerative and cardiovascular disorders, as well as cancer.

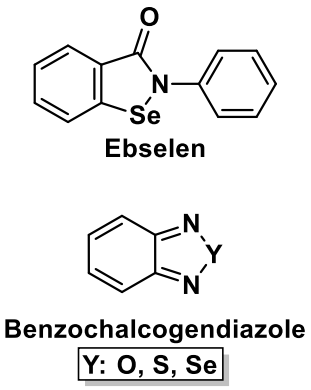

Figure 2. Structures of the clinical drug Ebselen and the bicyclic benzochalcogendiazole scaffold exploited in this work.

TDO2 is an emerging target in cancer immunotherapy primarily expressed in the liver and regulates L-Tryptophan's blood level. In oncology, tryptophan 2, 3-dioxygenase (TDO2) expression is especially important in liver, bladder, colon and pancreatic carcinomas.[31,32] TDO2 is also highly expressed in glioblastomas and melanomas.[31,33] TDO2 catalyzes L-Trp's oxidative cleavage into N-formylkynurenine, leading to L-Trp depletion and the increase in kynurenine levels. These two phenomena result in the suppression of effector T-cells and the induction of regulatory T-cells, leading to the arrest of the immune response and more aggressive and invasive tumors.[31,34–36] In the present work, we set out to study the equivalence of benzochalcogendiazole replacement in a small series of novel TDO2 inhibitors. These compounds were designed to optimize our benzotriazole-based TDO2 inhibitors reported earlier in 2021.[37] In the present study, we replaced the benzotriazole with benzochalcogendiazole moieties (**Figure 3**). Firstly, we hypothesized that 5-(1H-indol-3-yl)benzo[*c*][1,2,5]oxadiazole (**1**) could be accommodated in the enzymatic cavity by potentially forming a hydrogen bond with Arg-144 (**Figure 4**). Based on positive results with **1**, we next decided to study the impact of O isosteric replacement by S (**2**, **2*p***) or Se (**3**, **3*p***) on inhibitory potency and selectivity against IDO1, lipophilicity, microsomal stability and cellular toxicity.

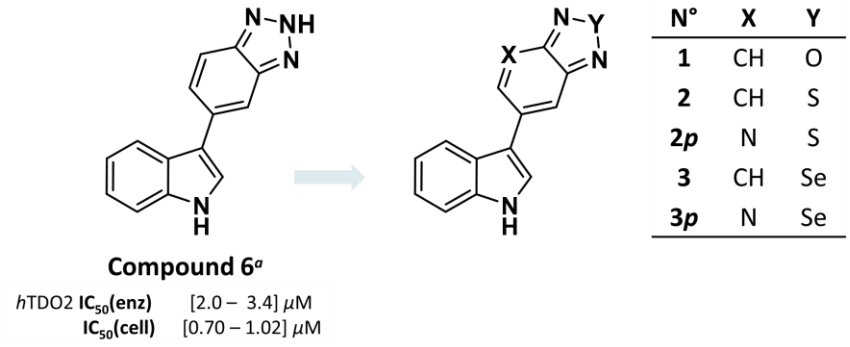

N°	X	Y
1	CH	O
2	CH	S
2*p*	N	S
3	CH	Se
3*p*	N	Se

Figure 3. On the left, [a] the previously reported 5-(1H-indol-3-yl)-benzotriazole.[37] On the right, analogs synthesized and evaluated as TDO2 inhibitors displayed in the present work.

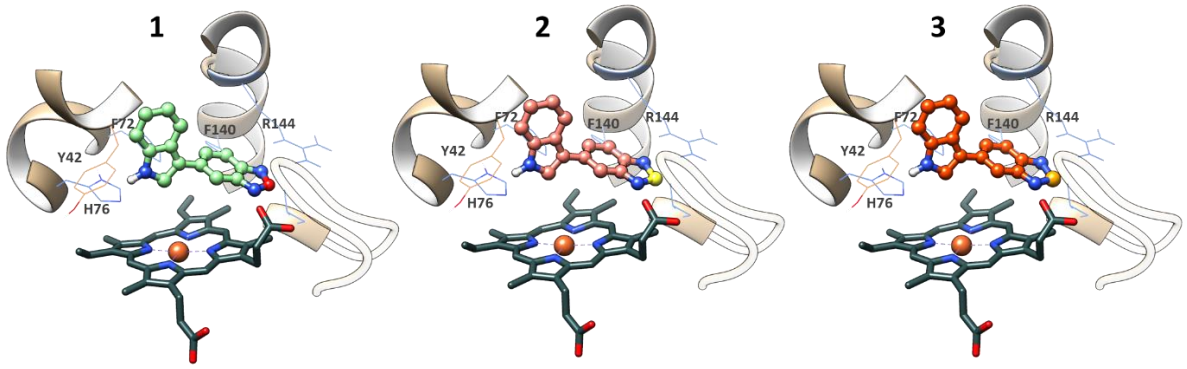

Figure 4. Molecular modeling of **1** (green-oxygen), **2** (pink-sulfur), **3** (red-selenium) inside TDO2 pocket (PDB structure: 5TI9)[38] shows the same pose for the three isomers. The chalcogen atoms are represented to scale. Selenium atom was treated with the same parameters as for sulfur in the present molecular docking. Therefore, the molecular docking of **3** only serves an illustrative purpose. The H-bond between Arg144 and compounds **1**, **2**, **3** were omitted for clarity. No H-bond was observed between the indole NH and H76 in agreement with our previous observations with the parent benzotriazole compound on TDO2.[36]

2. Results and discussion

2.1. Synthesis

All final compounds were synthesized by a Suzuki-Miyaura type cross-coupling between an aryl bromide and the appropriate boronic ester. Firstly, the thiadiazole derivatives **6** and **7** (**Scheme 1**, **a – b**) and selenadiazoles **8** and **9** (**Scheme 1**, **c – d**) were prepared starting from the commercially available

4-bromo-1, 2-diaminobenzene (**4**) and 5-bromopyridine-2,3-diamine (**5**). 5-bromobenzoxadiazole was purchased from a commercial source. The obtained aryl bromides were then used to perform the synthesis of cross-coupled products.

Scheme 1. Synthesis of 5-bromobenzochalcogendiazoles (6 – 9) [a]

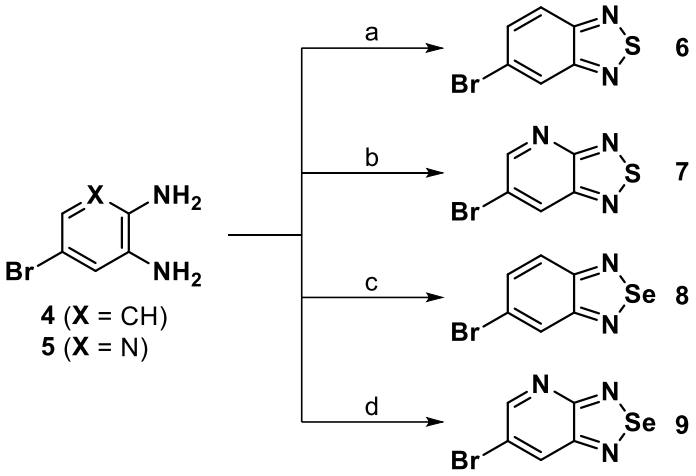

[a]Reagents and conditions: (a) $SOCl_2$, H_2SO_4, atm, 2 h, reflux. Yield: 80 % ; (b) $SOCl_2$, toluene/DMF, atm, overnight, reflux. Yield: 77 %; (c) SeO_2, EtOH, atm, 10 min reflux. Yield: quantitative ; (d) SeO_2, 5 min, Yield: quantitative.

Surprisingly, we could not apply the same synthetic route to obtain all final molecules, as we found significant differences in the reactivity during either the cross-coupling reaction or the final deprotection of the indole nitrogen. Indole boronates are known for being intrinsically unstable due to fast protodeboronation.[39,40] Therefore, we used two different boronic esters in the present work. In accordance with our previous experience of coupling reactions with indoles, we started all synthetic attempts with 1-(phenylsulfonyl)indole-3-boronic acid pinacol ester (**10**). This boronic ester is air-stable, inexpensive, easily accessible synthetically and, usually allows better yields in our optimized conditions than the indole protected with a Boc group.

Starting from **10** and 5-bromo-2,1,3-benzoxadiazole, we obtained (5-(1-(phenylsulfonyl)-1H-indol-3-yl)benzoxadiazole) following the optimized procedure with an 80 % yield (**Scheme 2**). Finally, deprotection in strong basic conditions using potassium hydroxide afforded final compound **1** with an overall yield of 80 %.

We next applied the same procedure to the synthesis of aryl-thiadiazole compounds **2** and ***2p***. However, we noticed that while the cross-coupled product was formed, it readily degraded during phenylsulfonyl deprotection in strong basic conditions. We also evaluated milder conditions that all resulted in the same degradation (e.g. 1M TBAF in THF). Thus, we decided to modify the boronate derivative in a way that would require acidic deprotection conditions. We chose Boc as the new protecting group and simultaneously tried two different routes (**Scheme 3**), both of which were successful.

Scheme 2. Synthesis of 5-(1H-indol-3-yl)benzoxadiazole (1) [a]

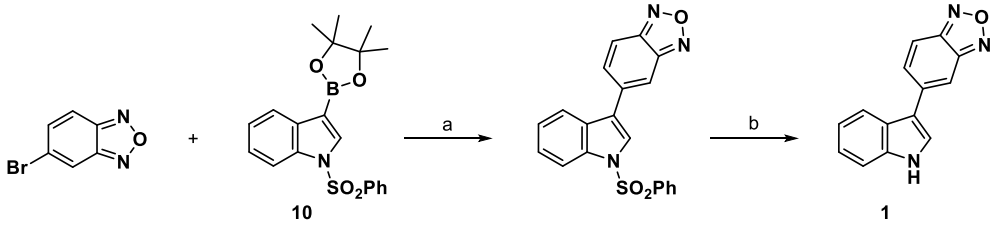

[a] Reagents and conditions: (a) 5-bromo-2,1,3-benzoxadiazole (1 eq.), **10** (1.2 – 1.5 eq.), 5 mol % $Pd(dppf)Cl_2$, 10 mol % SPhos, K_3PO_4 (2.0 eq), Dioxane/H_2O (5:1), 60°C, 3h, Under N_2; (b) KOH 2.5M in in MeOH/H_2O (1:1), reflux, overnight. Yield over two steps: 80 %.

Scheme 3. Synthesis of 5-(1H-indol-3-yl)benzothiadiazole (2) and 6-(1H-indol-3-yl)-[1,2,5]thiadiazolo[3,4-*b*]pyridine (*2p*). [a]

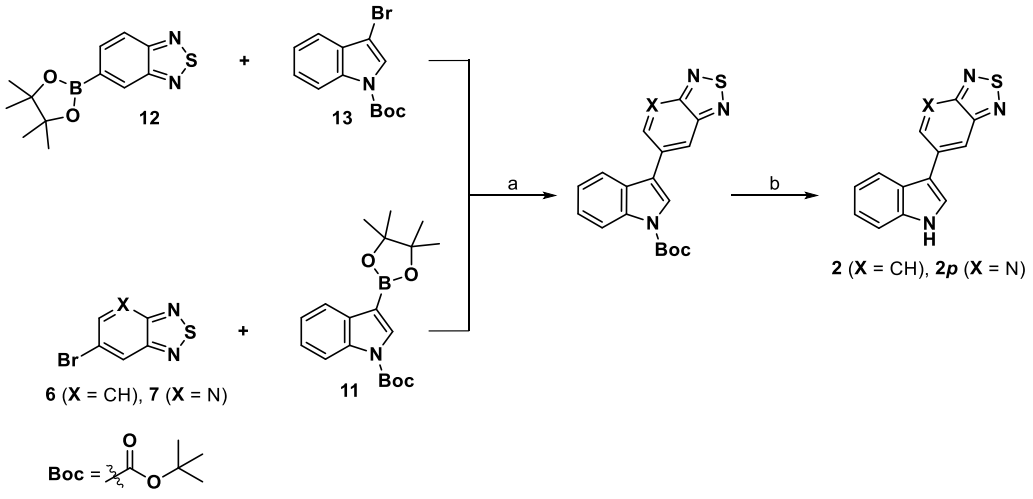

[a]Reagents and conditions: (a) Boronic ester (**11**/**12**) (1.2 – 1.5 eq.), 5 mol % $Pd(dppf)Cl_2$, 10 mol % SPhos, K_3PO_4 (2.0 eq), Dioxane/H_2O (5:1), 60°C, 3h, Under N_2; (b) HCl 4.0 M in MeOH/H_2O (1:1), reflux, overnight. Yield over two steps: **2**: 76 %, ***2p***: 42 %.

Finally, we applied the synthetic pathway of compound **1** to synthesize the Se analogs **3** and ***3p***. However, we did not detect the formation of a cross-coupling product under these conditions. Thus, we decided to modify the nature of the boronic ester and selected the MIDA ester boronate. MIDA boronates can slowly release the boronic acid compared to other esters, thus resolving the potential loss in reaction yield due to protodeboronation.[40] There are no available data regarding the reactivity of aryl benzoselenadiazoles derivatives in Suzuki-Miyaura couplings. Using the MIDA boronate **14**, we obtained the cross-coupled compounds **3** and ***3p*** with a high yield of 90 % of the pure compound after flash chromatography. We performed the deprotection in strong basic conditions and obtained the deprotected final compound in quantitative yield for **3** and around 40 % for ***3p*** due to loss during purification (**Scheme 4**).

Scheme 4. Synthesis of 5-(1H-indol-3-yl)benzoselenadiazole (3) and 6-(1H-indol-3-yl)-[1,2,5]selenadiazolo[3,4-b]pyridine (*3p*) [a]

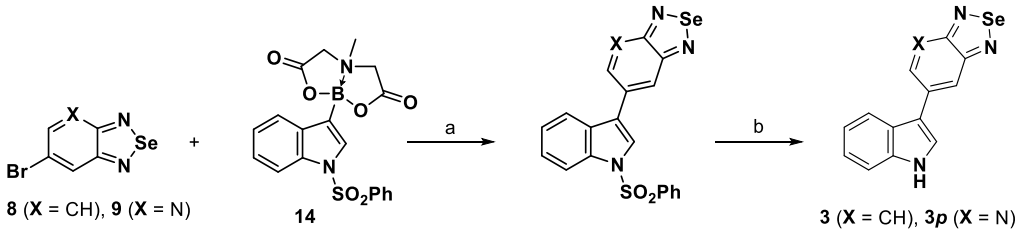

[a]Reagents and conditions: (a) Boronic ester (**14**) (1.2 eq), 5 mol % $Pd(dppf)Cl_2$, 10 mol % SPhos, K_3PO_4 (7.0 eq), Dioxane/H_2O (5:1), 60°C, 3h, Under N_2; (b) HCl 4.0 M in MeOH/H_2O (1:1), reflux, 1h. Yield over two steps: **3**: 79 %, ***3p***: 34 %.

2.2. Evaluation of Tryptophan 2, 3-dioxygenase inhibition, lipophilicity parameters and microsomal stability.

Next, we evaluated the synthesized isosteric inhibitors **1**, **2** and **3** and the two aza-analogs **2*p*** and **3*p*** in enzymatic and cellular assays for their ability to inhibit TDO2. The selectivity of these compounds towards TDO2 was also evaluated by performing the same assays against indoleamine 2,3-dioxygenase (IDO1), which presents a similar active site .[41] Overall, cellular and enzymatic IC_{50} indicated similar

activities against TDO2, demonstrating that affinity loss did not occur following the chalcogen replacement (**Figure 5,** CI95% IC_{50} values in **Table 1**). S to Se replacement even allowed a slight affinity gain even though lipophilicity decreased between **2** and **3**. Indeed, in lipophilic pockets such as the one of TDO2, a rise in lipophilicity usually results in more potent compounds due to better hydrophobic complementarities.

It should also be noted that the compounds reported here display the same inhibition characteristics as the previously published benzotriazole series, with a higher cell-based inhibition than enzymatic inhibition. As suggested in our previous work, different hypotheses could account for this difference, such as (i) an enzymatic assay which might poorly mimic the physiological redox state of TDO2 or (ii) binding of these compounds to apoTDO2, which would result in higher inhibition in cells than on the purified enzyme.[37]

Interestingly, none of the compounds could inhibit IDO1 (**Table 1**), suggesting that the observed inhibition of TDO2 did not stem from a non-specific effect, such as oxidation of the heme prosthetic group or by unspecific binding. Of note, the latter mechanism was reported for Ebselen, which inhibits IDO1 by binding to several cysteine residues with an apparent inhibition constant of 94 +/- 17 nM.[42,43]

We next evaluated the impact of chalcogen substitution on lipophilicity. Very few lipophilicity-related experimental data are available for Se species, leading to potentially unreliable software predicted data. Such data are of great importance for the future discovery of novel drug-like Se compounds in medicinal chemistry. In a recent paper, the replacement of an OCF_3 moiety by SCF_3 or $SeCF_3$ resulted in a 0.5 logP-units increase in lipophilicity.[26] In another example of rhodamine derivatives, integration of Se in some cases led to slightly more hydrophilic compounds, while opposite effects were also observed on similar scaffolds.[23] Thus, chalcogen replacement could prove helpful to modulate physicochemical properties and hence ADME parameters but still need further exemplification.[26] To evaluate the impact of chalcogen replacement on lipophilicity, we performed an experimental determination of Log K_w and compared them to calculated LogP values using the Chemicalize

(ChemAxon) and ACD/Percepta (Advanced Chemistry Development, Inc) softwares. Determining the Log K_w index using reversed-phase high-performance liquid chromatography (RP-HPLC) is a rapid and convenient method to estimate a molecule's lipophilicity. Log K_w is performed by measuring a compound's retention time in multiple methanol/water mobiles phases (isocratic elution) on a C18 silanized silica gel column. The obtained retention values form a linear regression curve of which Log K_w is the intercept (Supplementary data, **Figure S1**). Log K_w values usually have a very good correlation with the LogP value.[44–46] Moreover, because we compare a discrete substitution on an identical scaffold, we expect that the measured Log K_w values would only be influenced by the single modified atom, which will allow for a direct comparison between the compounds' lipophilicities.

We expected **1** to be the least hydrophobic compound due to its usually better capacity for hydrogen bonding. However, compounds **1** and **2** presented similar Log K_w values of respectively 4.1 and 4.0. Surprisingly, Se compounds resulted in drop of around 0.4 – 0.5 LogK_w-units of lipophilicity in **3** (Log K_w= 3.5) and ***3p*** (Log K_w= 2.9) compared to their S analogs **2** (Log K_w= 4.0) and ***2p*** (Log K_w= 3.3). This confirms that chalcogen replacement is a valid strategy to modulate the compound's lipophilicity but suggests that an increase in chalcogen size does not systematically lead to an increase in lipophilicity. While a reduction in hydrophobicity was previously observed following the replacement of sulfur by selenium,[23] it is worth mentioning that the impact on hydrophobicity appears much stronger in this benzochalcogendiazole series.

Interestingly, we found that the chalcogen atom replacement also had a significant impact on the microsomal stability. Indeed, Se compound **3** was the most stable, with a half-life between 70.2 and 100.8 minutes, while the least stable was O compound **1**. Pyridine analogs **2*p*** and **3*p*** showed a decrease of half-life compared to their parent compounds.

Table 1. Enzymatic and cellular inhibition values on TDO2 and experimentally determined Log K_{mw} (methanol/water), calculated LogP and microsomal stability half-lives.

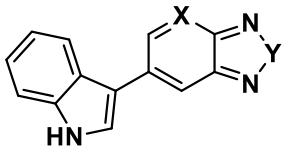

N°	X	Y	TDO2 IC_{50}[a] (μM) Enz.	TDO2 IC_{50}[a] (μM) Cell.	IDO1 IC_{50}[a] (μM) Enz. / Cell.	Log K_w[b]	*c*LogP[c]	Microsomal stability half-life (min.)
1	CH	O	[3.4 – 5.6]	[0.051 – 0.088]	> 100	4.1	3.41 (3.07)	[24.6 – 28.1]
2	CH	S	[3.0 – 4.9]	[0.129 – 0.199]	> 100	4.0	3.64 (3.86)	[35.6 – 50.1]
2p	N	S	[4.7 – 8.0]	[0.082 – 0.147]	> 100	3.3	2.83 (2.97)	[22.0 – 45.0]
3	CH	Se	[2.5 – 3.7]	[0.094 – 0.133]	> 100	3.5	3.10 (3.67)	[70.2 – 100.8]
3p	N	Se	[4.5 – 5.9]	[0.171 – 0.271]	> 100	2.9	2.36 (2.83)	[28.3 – 47.6]

[a] Reported 95 % confidence intervals IC_{50} values are calculated from measurements in triplicate. [b] Log K_w were obtained in two separate experiments [c] *c*LogP were calculated using ACD/Percepta 14.1.0 and Chemicalize (values reported in parenthesis).[47,48] [d] Reported 95 % confidence intervals for microsomal half-life were obtained in duplicates in two separate experiments. The error between two independent determinations is < 0,05 Log K_w unit. Traces and raw data of Log K_w and traces of microsomal half-lives can be found in supporting information (**Figure S1** and **S2**).

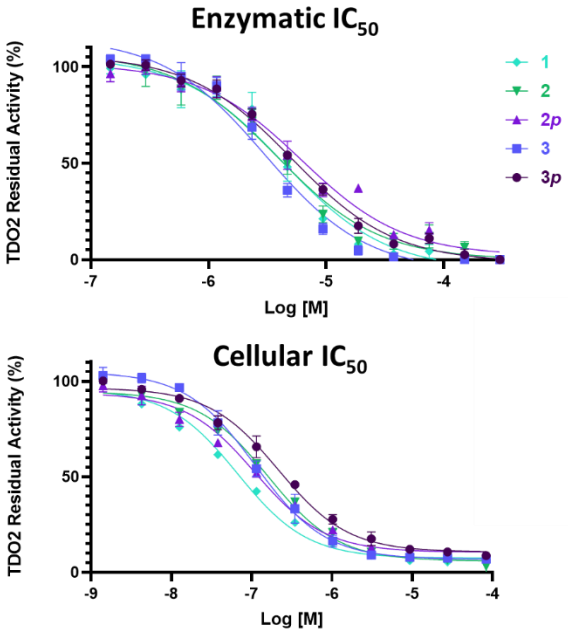

Figure 5. IC_{50} curves of inhibitors on TDO2. Data was obtained in quadruplicates in at least two separate experiments and analyzed with GraphPad Prism 8.

2.3. Evaluation of cellular toxicity and ROS induction

Next, we evaluated the cellular toxicity of the synthesized analogs on three different TDO2 expressing cell lines using an MTS assay. We used P815B murine mastocytoma cell line, A172 human glioblastoma cell line and human embryonic kidney 293 cells, HEK293 (**Table 2**). The assay was performed after 6h of exposition to assess whether compound exposure caused acute cell death. Furthermore, 6h is also the duration of an IC50 cellular assay on P815B cells. Additionally, we also performed the assay after 24h of exposition.

Compounds **1**, **2** and **3** all demonstrated similar toxicity patterns in the MTS assay. However, in few conditions (P815B (24h) and HEK293), compound **3** displayed slightly more toxicity than the other two chalcogen derivatives. On the other hand, compounds **2*p*** and **3*p*** displayed almost no toxicity and were only toxic on P815B cells after 24h treatment at high concentrations (above 30 µM, more than 150-fold $IC50_{cell}$ value). Interestingly, the presence of Se in **3*p*** did not influence the toxicity pattern. Following these results, we decided to use P815B cells to evaluate whether cells died from apoptosis or necrosis and if the Se-containing compounds were responsible for ROS elevation.

Table 2. Evaluation of toxicity on P815, A172 and HEK293 cell lines.

	LD50 (*µ*M)[a]					
	P815B		A172		HEK293	
	6h	*24h*	*6h*	*24h*	*6h*	*24h*
1	[10 – 30]	[10 – 30]	[30 – 80]	[30 – 80]	> 80	> 80
2	[30 – 80]	[10 – 30]	[30 – 80]	[30 – 80]	> 80	> 80
2*p*	> 80	[30 – 80]	> 80	> 80	> 80	> 80
3	[30 – 80]	[3 – 10]	[30 – 80]	[30 – 80]	[30 – 80]	[10 – 30]
3*p*	> 80	[30 – 80]	> 80	> 80	> 80	> 80

[a]Values obtained using the MTS assay, performed in triplicates. The curves can be found in supporting information (**Figure S3**).

Following 24h of treatment with 1 and 10 µM of inhibitors (as well as 5 µM for **3**), we next analyzed the cell death using Annexin V-FITC and propidium iodide (PI) staining followed with bi-parametric analysis by flow cytometry (FACS). As shown in **Figure 6a**, treatment with **3** at 10 µM caused an increase

of cells undergoing a late apoptotic/necrotic cell death (Annexin V+/PI+, **Figure 6b**), while the other analogs did not increase cellular death at 1 µM and 10 µM (**Figure 6a**).

The same experiment was performed using shorter treatment times to assess whether we could see an early apoptosis population. We did not observe any elevation of cell death after 3 hours of treatment with 10 μM of compound **3**. However, after 6 hours, 30.4 % of cells were dead, with 27.6 % in the double-positive square, suggesting a necrosis-type cell death (**Figure S4**).

To investigate the underlying mechanism of this observed toxicity, we evaluated the impact of a 24h treatment of 5 μM of **3** on cell cycle distribution of P815B cells using PI DNA staining. The FACS analysis revealed that incubation of cells with **3** did not result in an arrest of the cell cycle in G1 or G2 phases, thus further indicating a necrosis-type cell death (**Figure 6c**).

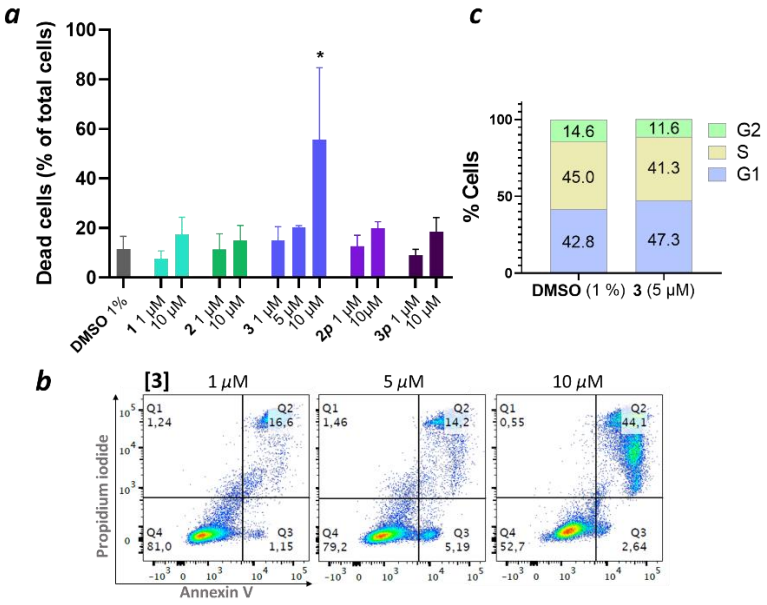

Figure 6. P815B cells were cultured with 1 to 10 µM of test compounds for 24h. Cells were double-stained with Annexin V-FITC/PI and analyzed by flow cytometry. The percentages correspond to Annexin V and/or PI positive cells (**a**). (**b**) Cell death induction by compound **3** in an Annexin V-FITC/PI assay (analyzed by flow cytometry) on P815B cells after 24h of treatment. (**c**) Bar diagram of cell distribution in different phases (G2, S, G1) of the cell cycle after 24h of treatment. At 5 μM, **3** had very little influence on cell viability and cell cycle. *P<0.05 in regard to the negative control.

As Se compounds are known for their redox capacities, we decided to investigate whether the observed toxicity of **3** could be attributed to oxidative stress. Therefore, we performed an H_2O_2 production assay in a cellular environment to evaluate whether the present scaffold could generate ROS (**Figure 7**). We measured a slight elevation of H_2O_2 levels at high concentrations of both **3** and the non-toxic analog **3*p***. Overall, these results suggest that, while compound **3** shows cellular toxicity at high concentration, this toxicity does not appear to be due to a non-specific redox effect of the Se as (i) the pyridine analog (**3*p***) does not exhibit any similar toxicity and (ii) the toxicity does not seem to arise from ROS generation.

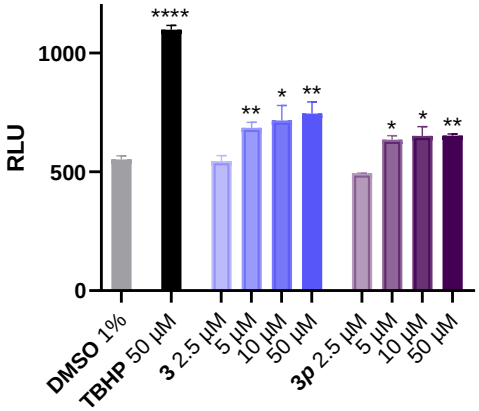

Figure 7. Production of ROS following treatment with Se compounds **3** and **3*p*** using the bioluminescent ROS-Glo™ H_2O_2 assay (Promega, USA). Data is shown in relative luminescence units (RLU). The assay was performed in triplicates in two separate experiments. ****P<0.0001, **P<0.005, *P<0.05 in regard to the negative control.

3. Conclusions

In the work herein, we designed, synthesized and compared isosteric replacement of O, S and Se aryl-chalcogendiazoles on TDO2 inhibitors. We showed that chalcogen replacement did not significantly impact TDO2 affinity and that introducing a Se did not lead to unspecific inhibition of IDO1, an enzyme with a similar active site. Interestingly, Se substitution influenced the compound's lipophilicity and microsomal stability. In the present case, the two Se compounds were the least lipophilic and presented the most stable. Se compound **3**, displayed more cellular toxicity than its O and S isosteres in all three evaluated cell lines. However, the observed toxicity occurred at a concentration close to

100 times above the IC_{50} value. Furthermore, this toxicity did not appear to be Se-related, as the second Se compound **3*p***, bearing a [1,2,5]selenadiazolo[3,4-*b*]pyridine instead of a benzo[*c*][1,2,5]selenadiazole, displayed the lowest toxicity in our experimental settings. Both Se compounds could only induce ROS at high concentrations, contrary to the common preconception regarding Se-containing molecules. These data suggest that liabilities observed at higher concentrations of **3**, may not be solely attributed to the presence of Se or that Se-related toxicity is heavily dependent on the scaffold. Overall, The introduction of Se in drug-like structures should thus be worthy of consideration in medicinal chemistry designs, and new data of Se containing scaffolds are crucial for future lipophilicity and ADME/Tox predictions. Regarding the chemistry, it would give more insights into their synthetic accessibility and reactivity. As of today, an increasing amount of publications seems to suggest that Se might someday be a part of the chemical drug space.

4. Experimental section

4.1. General experimental parameters

All reagents and starting materials were obtained from various commercial suppliers and used without any further purification. Progression of reactions was monitored using thin-layer chromatography (TLC) with silica gel 60 F_{254} coated aluminium sheets (Merck). Flash purification of compounds was performed using silica gel in glass columns with various gradients of ethyl acetate and cyclohexane. Final purity was assessed with an HPLC system to be above 95 % (Agilent (1100 series) HPLC single quadrupole (InfinityLab, ESI+) system equipped with a Kinetex 5 µm EVO C18 (150 mm × 4,6 mm) using a gradient of distilled water + 0.1% TFA (buffer A) and acetonitrile + 0.1% TFA (buffer B). HPLC conditions for purity analysis were 5% B + 95% A at a flow rate of 1 mL/min, followed by an increase of solution B to 80% in 15 min (5%/min). The wavelength for UV detection was 254 nm and 230 nm). HPLC purities of final compounds that underwent biological assessment were ≥ 95%, traces can be found in supporting information (**Figure S7**). Compounds were also analyzed in a UPLC Waters Class H system equipped with a Kinetex 2.6 um EVO C18 100A (2,1 X 50) column (Phenomenex) and were

eluted using a 3.0 min linear gradient of acetonitrile in water (5-50 %) containing 0.1 % trifluoroacetic acid at a flow-rate of 0,6 ml/min. UPLC and HPLC traces can be found in supporting information (**Figure S6** and **S7**). Characterization was performed with ^{1}H and ^{13}C NMR in either $CDCl_3$ or DMSO-*d6* (Eurisotop). Chemical shifts are in parts per million (ppm), coupling constants (J) are in hertz (Hz). Standard abbreviations indicating multiplicity were used as follows: s = singlet, d = doublet, t = triplet, dd = doublet of doublets, m = multiplet, br = broad. Representative NMR spectra for compounds **1**,**2** and **3** can be found on **Figure S5**. Melting points were determined using an electrothermal IA9000 apparatus and are reported uncorrected. $LogD_{7.4}$ calculations were performed using Chemicalize (ChemAxon).

4.2. General cross-coupling procedure

Prior to the coupling procedures, the solvent 1,4-Dioxane and K_3PO_4 solution in water were degassed by atmosphere exchange with nitrogen in a sonication bath for 45 minutes. Aryl-halide (1mmol, 1 eq) and the boronic ester (1.5 eq), $Pd(dppf)Cl_2$ (5 mol %) and SPhos (10 mol %) were introduced into a 25 ml 2-neck round-bottom flask under inert atmosphere. Then, 10 mL of degassed dioxane were added and the reaction was left under agitation at r.t. for 10 minutes until dissolution of reactants. Finally, 2 mL of degassed distilled water containing K_3PO_4 (3.5 mmol) were added to the media and the reaction was stirred for 3h at 60°C. When the conversion was complete, the mixture was cooled to room temperature, diluted with 1N NaOH (10 mL) and extracted twice with 10 mL EtOAc. The combined organic fractions were dried over Na_2SO_4 and concentrated in vacuo. This general procedure was slightly adapted when couplings were performed using MIDA boronate **14**. In this modified procedure 1.2 eq of boronate and 7 eq of K_3PO_4 were used.

4.3. General acidic and basic deprotection procedures

Around 0.5 mmol of starting compound were dissolved in 4 mL of a 1:1 solution of $MeOH/H_2O$ containing 2.5 M of **A)** KOH (for SO_{2p}h deprotection) or **B)** HCl (for Boc deprotection). The resulting mixture was refluxed until completion of the reaction (1h. – overnight). After completion, the reaction

mixture was cooled to room temperature and extracted with ethyl acetate. The organic layer was dried with Na_2SO_4 and concentrated in vacuo before being purified by flash chromatography using a gradient ethyl acetate in cyclohexane (1:4 ➔ 2:1).

4.4. Compound synthesis

4.4.1. Synthesis of 5-bromobenzo[c][1,2,5]thiadiazole (6).

An RB flask was charged with thionyl chloride (3.5 mL, 48.4 mmol, 9 eq.) and 4-bromo-1,2-diaminobenzene (1 g, 5.3 mmol, 1 eq.) was added portion wise. After the addition, 0.16 mL of concentrated sulfuric acid (0.54 eq.). The resulting mixture was agitated under reflux for 1.5 hours. After cooling to room temperature, the mixture was poured on ice, extracted with dichloromethane. The OL was dried with $MgSO_4$ and concentrated in vacuo. Yield: 80 %. ^{1}H RMN (400MHz, DMSO) : δ 7.85 (1H, dd, J=1.84, 9.25 Hz), 8.08 (1H, d, J=9.23 Hz), 8.47 (1H, d, J=1.31 Hz). ^{13}C RMN (100 MHz, DMSO): δ 123.04; 123.98; 124.53; 133.62; 153.37; 155.23.

4.4.2. Synthesis of 6-bromo-[1,2,5]thiadiazolo[3,4-b]pyridine (7)

The synthesis was performed according to a previously described procedure.[49] An RB flask was charged with 3 mL of toluene, dimethylformamide (50 µL) and 2,3-diamino-5-bromopyridine (0.5 g, 2.7 mmol) and heated to 70°C. Then, 1 mL of thionyl chloride were added and the final mixture was refluxed overnight at 90°C. After cooling down to room temperature, the precipitate was filtered and washed with H2O and ethanol to afford the desired compound. Yield: 77 %. ^{1}H RMN (400MHz, $CDCl_3$) : δ 8.56 (1H, d, J=1.54 Hz), 9.09 (1H, s). ^{13}C RMN (100 MHz, $CDCl_3$): δ 121.25; 131.28; 147.96; 156.89; 160.01.

4.4.3. Synthesis of 5-bromobenzo[c][1,2,5]selenadiazole (8).

A solution of 4-bromo-1,2-diaminobenzene (1.2 g, 6.4 mmol, 1 eq.) in ethanol (9 mL) was heated to reflux temperature and selenium dioxide (0.8 g, 7 mmol, 1.1 eq.) was added. The addition of selenium dioxide resulted in an immediate precipitation of the desired product. After 10 minutes of reflux, the reaction mixture was cooled to 0°C and the precipitate was filtrated and washed with H_2O.

Quantitative yield. ^{1}H RMN (400MHz, DMSO) : δ 7.66 (1H, dd, J=1.74, 9.42 Hz), 7.81 (1H, d, J=9.40 Hz), 8.19 (1H, d, J=1.25 Hz). ^{13}C RMN (100 MHz, DMSO): δ 124.59; 124.64; 125.52; 132.83 (1C, s), 158.56 (1C, s), 160.21 (1C, s).

4.4.4. Synthesis of 6-bromo-[1,2,5]selenadiazolo[3,4-b]pyridine (9).

6-bromo-[1,2,5]selenadiazolo[3,4-b]pyridine was synthesized following a previously described procedure.[29] *In a mortar,* 2,3-diamino-5-bromopyridine was ground with selenium dioxide for 5 minutes. Then the reaction mixture was heated to 90°C and the crude residue was washed with H_2O. Quantitative yield. ^{1}H RMN (400MHz, DMSO): δ 8.72 (1H, d, J=2.24 Hz), 9.09 (1H, d, J=2.24 Hz). ^{13}C RMN (100 MHz, DMSO): δ 120.78; 133.10; 153.37; 157.20; 162.65.

4.4.5. Synthesis of 3-bromo-1H-indole

Indole (1 g, 8.5 mmol) was dissolved in 100 mL of pyridine. After what, pyridinium tribromide (1.25 equi., 3.4 g., 10.6 mmol) in 100 mL pyridine was added dropwise using a dropping funnel and the reaction was left to stir for 1 hour. Next, ice water was added and the reaction mixture was extracted with Et_2O (3x). The organic layer (OL) was washed with 6N HCl and saturated $NaHCO_3$, dried with $MgSO_4$, filtered and concentrated *in vacuo* to afford 1.3 grams of a beige powder, which was used as such in the next step. Yield= 78 %. ^{1}H-NMR (400 MHz, $CDCl_3$): δ 14.27 (bs, 1H), 9.03 (d, J= 5.34 Hz, 2H), 8.56 (t, J= 7.82 Hz, 1H), 8.10 (t, J= 6.94 Hz, 2H).

4.4.6. Synthesis of 3-bromo-1-(phenylsulfonyl)-1H-indole

A 2-necked round bottom (RB) flask was charged with 3-bromo-1H-indole (1250 mg, 6.4 mmol) and TBAHS (3250 mg, 1 mmol) in 30 mL toluene at 0°C. Next, 30 mL of a aqueous NaOH 50 % solution and benzenesulfonyl chloride (1690 mg, 1.2 mL, 9.6 mmol) were added dropwise. The reaction mixture was left to stir at rt overnight. After TLC showed full conversion, the OL layer was separated, acidified with 1N HCl, neutralized with $NaHCO_3$, washed with brine, dried with Na_2SO_4 and concentrated in vacuo to be used as such. The product was obtained as a beige powder in quantitative yield. ^{1}H-NMR

(400 MHz, $CDCl_3$): δ 7.35 (1H, t, J=7.45 Hz), 7.41 (1H, t, J=7.32 Hz), 7.48 (2H, t, J=7.77 Hz), 7.53 (1H, d, J=7.82 Hz), 7.58 (1H, t, J=7.46 Hz), 7.66 (1H, s), 7.92 (2H, d, J=7.61 Hz), 8.03 (1H, d, J=8.29 Hz). ^{13}C NMR (100 MHz, $CDCl_3$): δ 136.52; 134.91; 133.55; 130.02; 129.07; 126.82; 126.15; 125.63; 124.47; 119.77; 113.45; 98.92.

4.4.7. 1-(phenylsulfonyl)-3-(4,4,5,5-tetramethyl-1,3,2-dioxaborolan-2-yl)-1H-indole (10)

A RB flask was charged with 3-bromo-1-(phenylsulfonyl)-1H-indole (1000 mg, 3 mmol), bis(pinacolato)diboron (1020 mg, 4 mmol) and KOAc (880 mg, 89.3 mmol) in 10 mL DMF. The reaction mixture was degassed for 20 min, after which Pd(dppf)Cl_2 (66 mg, 3 mol%) was added. The reaction was stirred at 80°C overnight. After TLC showed full conversion, EtOAc was added and the mixture was filtered over a pad of celite. The OL was evaporated in vacuo. The crude product was purified using flash chromatography (cyclohexane/EtOAc: 4/1) to obtain 800 mg of the desired product. Yield: 69 %. ^{1}H NMR (400 MHz, $CDCl_3$): δ 1.26 (12H, s), 7.30 (2H, t, J=7.38 Hz), 7.36 (1H, d, J=7.96 Hz), 7.42 (3H, t, J=7.85 Hz), 7.46 – 7.54 (3H, m, J=7.27 Hz), 7.63 (1H, s), 7.88 (2H, d, J=7.73 Hz), 8.00 (1H, d, J=8.31 Hz). ^{13}C NMR (100 MHz, $CDCl_3$): δ 25.04; 83.52; 99.84; 113.56; 120.11; 124.01; 124.72; 125.88; 126.85; 129.44; 134.18; 137.74.

4.4.8. Synthesis of 5-(4,4,5,5-tetramethyl-1,3,2-dioxaborolan-2-yl)benzo[c][1,2,5]thiadiazole (12)

A flame dried two-necked RB flask under N_2 atmosphere was charged with 5-bromobenzo[*c*][1,2,5]thiadiazole (**6**) (2 g, 9.3 mmol, 1 eq.), Bis(pinacolato)diboron (4.7 g, 18.6 mmol, 2eq.) and potassium acetate (3 g, 30 mmol, 3 eq.). Then, 60 mL of dry DMF were added. After 5 minutes, Pd(dppf)Cl_2 (5 mol %, 340 mg) was added and the reaction was left under agitation overnight, at 80°C. The conversion was total. The reaction mixture was filtered on a celite pad and the filtrate was extracted with ethyl acetate and water. The OL was concentrated and the residue was purified by flash chromatography in a cyclohexane/ethyl acetate gradient. Yield: 68 %. ^{1}H RMN (400MHz, DMSO) : δ

1.35 (12H, s), 7.86 (1H, d, J=8.80 Hz), 8.08 (1H, d, J=8.80 Hz), 8.34 (1H, s). ^{13}C RMN (100 MHz, DMSO): δ 25.14; 84.87; 121.39; 128.95; 133.84; 154.39; 155.95.

4.4.9. Synthesis of tert-butyl 3-bromo-1H-indole-1-carboxylate (13)

To a 0.1 M solution of *3-bromo-1H-indole* (6,97g, 29,62mmol, 1eq) in dichloromethane was added N-bromosuccinimide (NBS) (6.85g, 38.50 mmol, 1.1 equi). The solution was stirred at atm. P. under reflux for 6h. 0.1 equi of NBS were added after 2h, 4h, and 5h. If added all at once, this leads to the formation of a dibrominated compound. The reaction mixture was subsequently washed with H_2O, 1M NaOH and Brine, dried with $MgSO_4$ and concentrated in-vacuo. The obtained residue was crystallized in EtOH. Pink crystals. Yield: 80 %. ^{1}H RMN (400MHz, $CDCl_3$) : δ 1.69 (9H, s), 7.08 (1H, td, J=8.81Hz, J=1.9Hz), 7.47 (1H, dd, J=8.56Hz, J=5.3Hz), 7.63 (1H, s), 7.91 (1H, s). ^{13}C RMN (100 MHz,$CDCl_3$): δ 28.11 ; 84.77 ; 97.59 ; 102.84 (d, J=29.07 Hz) ; 111.69 (d, J=24.70 Hz) ; 120.43 (d, J=10.03 Hz) ; 125.04 ; 125.74 ; 134.72 (d, J=11.67 Hz) ; 148.63 ; 161.57 (d, J=241.79 Hz).

4.4.10. Synthesis of 4-methyl-8-(1-(phenylsulfonyl)-1H-indol-3-yl)dihydro-4l4,8l4-[1,3,2]oxazaborolo[2,3-b][1,3,2]oxazaborole-2,6(3H,5H)-dione (14)

The synthesis was adapted from a previously described procedure.[40] To a RB flask equipped with a stir bar, was added the commercially available 1-(phenylsulfonyl)-3-indoleboronic acid (1 eq, 1 g, 3.32 mmol), N-methyliminodiacetic acid (1.5 eq, 0.732 g, 4.96 mmol), toluene (21 mL) and DMSO (11 mL). The flask was fitted with a Dean-Stark trap connected with a reflux condenser vented to ambient atmosphere. The stirred mixture was heated to reflux for 1h30 until reaction completion. Then, toluene was evaporated in vacuo. The desired product (**14**) was precipitated with cyclohexane and filtered over a glass filter funnel. The final compound was obtained as a white powder with a yield of 85 %. ^{1}H RMN (400MHz, $CDCl_3$) : δ 2.56 (3H, s), 4.19 (2H, d, J=17.21 Hz), 4.39 (2H, d, J=17.25 Hz), 7.22 – 7.29 (1H, d, J=26.01 Hz), 7.32 (1H, t, J=7.62 Hz), 7.52 – 7.63 (3H, m), 7.69 (1H, t, J=7.30 Hz), 7.74 (1H, s), 7.90 (1H, d, J=8.16 Hz), 8.03 (2H, d, J=7.80 Hz). ^{13}C RMN (100MHz, $CDCl_3$) : δ 47.76; 62.29; 113.51; 122.77; 123.94; 124.81; 127.27; 130.26; 132.54; 133.83; 135.10; 135.63; 137.40.

4.4.11. Synthesis of 5-(1H-indol-3-yl)benzo[c][1,2,5]oxadiazole (1)

The cross-coupled product was synthesized following the general coupling procedure using 5-bromo-2,1,3-benzoxadiazole (purchased from Fluorochem) and 1-(phenylsulfonyl)-3-(4,4,5,5-tetramethyl-1,3,2-dioxaborolan-2-yl)-1H-indole (**10**). Following the coupling, the resulting crude was filtrated through a silica pad and eluted with 1:4 mixture of ethyl acetate/cyclohexane. After concentration in vacuo, the residue containing the protected intermediate (*5-(1-(phenylsulfonyl)-1H-indol-3-yl)benzo[c][1,2,5]oxadiazole* ^{1}H RMN (400MHz, DMSO) : δ 7.40 (1H, t, J=7.30 Hz), 7.47 (1H, t, J=7.48 Hz), 7.62 (1H, t, J=7.20 Hz), 7.72 (1H, t, J=6.88 Hz), 7.93 (1H, d, J=9.20 Hz), 8.00 (1H, t, J=8.88 Hz), 7.90 – 8.09 (4H, m), 8.10 – 8.21 (3H, m), 8.44 (1H, s))

underwent general deprotection procedure **A** overnight to afford **1**. Yield over two steps: 80 %. ^{1}H RMN (400MHz, $CDCl_3$) : δ 7.28 – 7.31 (1H, m,), 7.32 – 7.35 (1H, m), 7.50 (1H, d, J=7.98 Hz), 7.59 (1H, d, J=2.67 Hz), 7.79 (1H, dd, J=1.37, 9.30 Hz), 7.87 (1H, dd, J=0.94, 9.30 Hz), 8.02 (1H, d, J=7.98 Hz), 8.06 (1H, t, J=0.99 Hz), 8.49 (1H, s). ^{13}C RMN (100 MHz, DMSO): δ 109.94; 111.90; 116.37; 116.42; 119.78; 121.44; 123.38; 123.84; 125.11; 133.68; 136.90; 138.55; 148.42; 150.05. HRMS: m/z (EI+), calculated for: $C_{14}H_9N_3O$ 236.0818 $[M+H]^+$, found: 236.0815 $[M+H]^+$.Melting range: 195.6 – 199.8 °C.

4.4.12. Synthesis of 5-(1H-indol-3-yl)benzo[c][1,2,5]thiadiazole (2)

The cross-coupled product was synthesized following the general coupling procedure using 5-bromobenzo[*c*][1,2,5]thiadiazole (**6**) and 3-Bpin-N-Boc-indole **11** (Fluorochem). Following the coupling, the resulting crude was filtrated through a silica pad and eluted with 1:3 mixture of ethyl acetate/cyclohexane. After concentration in vacuo, the residue underwent general deprotection procedure **B** overnight to afford **2**. Yield over two steps: 76 %. ^{1}H RMN (400MHz, $CDCl_3$) : δ 7.28 (1H, t, J=7.41 Hz), 7.32 (1H, t, J=7.44 Hz), 7.49 (1H, d, J=7.98 Hz), 7.58 (1H, d, J=2.22 Hz), 7.97 (1H, dd, J=1.05, 9.03 Hz), 8.04 (1H, d, J=9.06 Hz), 8.07 (1H, d, J=7.86 Hz), 8.29 (1H, s), 8.43 (1H, s). ^{13}C RMN (100 MHz, $CDCl_3$) : δ 111.71; 116.89; 117.08; 119.82; 121.08; 121.35; 123.05; 123.21; 125.40; 131.04; 136.88;

137.07; 153.78; 155.82. HRMS: m/z (EI+), calculated for: $C_{14}H_9N_3S$ 252.0590 $[M+H]^+$, found: 252.0580 $[M+H]^+$. Melting range: 183.1 – 183.6 °C.

4.4.13. Synthesis of 6-(1H-indol-3-yl)-[1,2,5]thiadiazolo[3,4-b]pyridine (2p)

The cross-coupled product was synthesized following the general coupling procedure using 6-bromo-[1,2,5]thiadiazolo[3,4-*b*]pyridine (**7**) and 3-Bpin-N-Boc-indole. Following the coupling, the resulting crude was filtrated through a silica pad and eluted with 1:1 mixture of ethyl acetate/cyclohexane. After concentration in vacuo, the residue underwent general deprotection procedure **B** overnight to afford ***2p***. Yield over two steps: 42 %. ^{1}H RMN (400MHz, DMSO) : δ 7.23 (1H, t, J=7.31 Hz), 7.27 (1H, t, J=7.36 Hz), 7.55 (1H, d, J=7.68 Hz), 8.11 (1H, d, J=7.62 Hz), 8.29 (1H, s), 8.66 (1H, s), 9.64 (1H, s), 11.86 (1H, s). ^{13}C RMN (100 MHz, DMSO): δ 111.48; 112.87; 119.81; 121.25; 121.62; 122.86; 125.21; 127.42; 133.19; 137.64; 148.58; 157.80; 159.94. HRMS: m/z (EI+), calculated for: $C_{13}H_9N_4S$ 253.0542 $[M+H]^+$, found: 253.0545 $[M+H]^+$. Melting range: 241.6 – 243.1 °C.

4.4.14. Synthesis of 5-(1H-indol-3-yl)benzo[c][1,2,5]selenadiazole (3)

The cross-coupled product was synthesized following the general coupling procedure using 5-bromobenzo[*c*][1,2,5]selenadiazole (**8**) and 1-(phenylsulfonyl)-3-indolylboronic acid MIDA ester (**14**). Following the coupling, the resulting crude was filtrated through a silica pad and eluted with 1:1 mixture of ethyl acetate/cyclohexane. After concentration in vacuo, the residue was triturated in cyclohexane and the obtained precipitate was filtrated before undergoing general deprotection procedure **B** for 1h to afford **3**. Yield over two steps: 79 %. ^{1}H RMN (400MHz, $CDCl_3$) : δ 7.27 – 7.35 (2H, m), 7.49 (1H, d, J=7.68 Hz), 7.60 (1H, d, J=2.44 Hz), 7.86 (1H, s), 8.09 (1H, d, J=7.64 Hz), 8.14 (1H, s), 8.47 (1H, s). ^{13}C RMN (100 MHz, DMSO): δ 111.73; 116.58; 118.35; 120.09; 121.14; 123.11; 123.19; 123.37; 125.36; 131.39; 136.95; 136.98; 159.74; 161.46. HRMS: m/z (EI+), calculated for: $C_{14}H_9N_3Se$ 300.0034 $[M+H]^+$, found: 300.0037 $[M+H]^+$. Melting range: 206.7 – 210.2

4.4.15. Synthesis of 6-(1H-indol-3-yl)-[1,2,5]selenadiazolo[3,4-b]pyridine (3p)

The cross-coupled product was synthesized following the general coupling procedure using 6-bromo-[1,2,5]selenadiazolo[3,4-*b*]pyridine (**9**) and 1-(phenylsulfonyl)-3-indolylboronic acid MIDA ester (**14**). Following the coupling, the resulting crude was filtrated through a silica pad and eluted with 1:1 mixture of ethyl acetate/cyclohexane. After concentration in vacuo, the residue was purified by flash chromatography (ethyl acetate/cyclohexane, 1:2 ➔ 1:0) to afford the protected intermediate *6-(1-(phenylsulfonyl)-1H-indol-3-yl)-[1,2,5]selenadiazolo[3,4-b]pyridine* ^{1}H RMN (400MHz, DMSO) : δ 7.39 – 7.54 (2H, m), 7.59 – 7.77 (3H, m), 8.07 (2H, dd, J=7.72, 15.89 Hz), 8.16 (2H, d, J=6.52 Hz), 8.59 (1H, s), 8.66 (1H, s), 9.54 (1H, s). The protected intermediate underwent general deprotection procedure **B** for 1h to afford ***3p***. Yield over two steps: 34 %. ^{1}H RMN (400MHz, DMSO) : δ 7.23 (1H, t, J=6.96 Hz), 7.26 (1H, t, J=7.02 Hz), 7.54 (1H, d, J=7.98 Hz), 8.09 (1H, d, J=7.80 Hz), 8.30 (1H, s), 8.38 (1H, d, J=2.40 Hz), 9.58 (1H, d, J=2.40 Hz), 11.86 (1H, s). ^{13}C RMN (100 MHz, DMSO): δ 111.34; 112.88; 119.94; 121.22; 122.45; 122.86; 125.22; 127.42; 132.10; 137.69; 154.02; 158.59; 162.94. HRMS: m/z (EI+), calculated for: $C_{13}H_9N_4Se$ 300.9987 $[M+H]^+$, found: 300.9995 $[M+H]^+$ Melting range: 263.1 – 267.4 °C.

4.5. Enzyme production and purification

TDO2 was produced using our previously described procedure.[37] The recombinant plasmid coding for the truncated version of *h*TDO2 was transferred into the E. coli strain BL21 (DE3) (Rosetta). The selected transformed single colony was used to inoculate an LB medium (50 µg/mL kanamycin and 34 µg/mL chloramphenicol). Cells were cultured at 37 °C until an optical density of 0.6 was reached. The expression of *h*TDO2 was induced by isopropyl 1-thio β galacto-pyranoside (IPTG) (final concentration of 1 mM). An aliquot of hemin in NaOH 0.5M (final concentration of 8–10 µM) was added to the culture. The culture was grown at 20 °C for 20 h. Cells were harvested by centrifugation at 5000 rpm, 4 °C for 25 min. Cell pellets were resuspended in a lysis buffer (Tris-HCl 50 mM, pH 8.5, MgCl2 10 mM, NaCl 300 mM, imidazole 5 mM, and glycerol 10%) supplemented with protease inhibitors (Roche) and then disrupted by sonication, followed by centrifugation at 4 °C, 10 000 rpm for 30 min. The supernatant was collected, and 1 µL/mL of supernatant of β-mercaptoethanol was added before

loading onto 1 mL of His-trap FF-crude columns (GE Healthcare). Protein concentrations were measured using the Bradford method with the Biorad protein assay kit, and sample homogeneity was assessed using sulfate−polyacrylamide gel electrophoresis (SDS−PAGE) with Coomassie brilliant blue as a staining agent. Finally, purified *h*TDO2 was dialyzed overnight in a pH 7.6 buffer containing 50mM sodium phosphate, 100mM NaCl, 20% glycerol and 10mM L-Trp.

4.6. Enzymatic IC_{50} determination

The assay was performed in a pH 6.5 potassium phosphate buffer (100 mM) at 37°C. The final concentrations in each well were: 100 µM of L-Trp, 20 mM of L-ascorbate, 10 µM of methylene blue, 150 nM of catalase, 3 % of DMSO containing the inhibitor and 0.01 % v/v of Triton X-100. The assay was initiated by adding 15 µL of buffer containing approximately 80 nM of *h*$TDO2_{tr}$ (no L-Trp, no DMSO) to 85 µL of buffer (with L-Trp and the tested inhibitor concentration in DMSO). After 15 minutes, 20 µL 30 % m/v of trichloroacetic acid (TCA) in water were added and the plates were heated at 65°C for 15 minutes. Then, 100 µL of a 2% m/v p-dimethylbenzaldehyde solution in pure acetic acid was added to each well. After 10 minutes, absorbance reading was performed at 490 nM.

For testing against IDO1, 30 nM of purified *h*IDO1 were used, and the incubation time was shortened to 8 minutes before quenching with TCA to remain under initial velocity conditions.

4.7. Cell Culture Conditions

P815B, HEK293 and A172 cell lines were maintained in IMDM medium supplemented with 10% fetal bovine serum (FBS), 1x GlutaMAX and 1x Pen/Strep, at 37 °C and 5% CO_2.

4.8. Cellular IC_{50} determination

The assay was performed in 96-well flat-bottom plates seeded with 1×10^5 cells (P815B-hTDO2, clone 19) in a final volume of 200 μL of Iscove's modified Dulbecco medium (80 mmol/L Trp) supplemented with 2% FCS in the presence of the TDO inhibitor at different concentrations (1–25,000 nM) for 7 hours when substrate consumption was below 25 %. Cells were centrifuged 10 min at 300 RCF, after which

60 μL of supernatant were collected and mixed with 60 μL of 12% (wt/vol) trichloroacetic acid. After centrifugation at 4°C, 23000 RCF, 70 μL of supernatant was diluted with 70 μL of HPLC grade H_2O. The resulting solution was used to quantify L-Trp and L-Kyn concentrations by ultra-performance liquid chromatography (UPLC) based on the retention time and the UV absorption.

The same protocol was applied for hIDO1 counter-screening (P815B-*h*IDO1), but the plates were seeded with 2 × 105 cells and incubated for 24h to achieve a similar L-Trp consumption.

4.9. Cell viability assay

The effect of the compounds on cancer cell viability was determined by the MTS assay uptake method. Briefly, after incubation for the appropriate amount of time (6 and 24h), 21 μL (20 μL of PMS and 1 μL of MTS) were added to well containing the cells in 200 μL in DMEM containing 5% of FBS and different concentrations of test compounds in triplicates (HEK293 cells were seeded at 30.000 cells/well, A172 at 20.000 cells/well and P815B at 50.000 cells/well). Then, the cells were incubated until complete development of the coloration (usually around 2 to 4 hours) at 37 °C, absorbance at 490 nm was measured. Graphpad Prism software was used to calculate the residual viability of cells.

4.10. Annexin V/PI Assay

TDO2-expressing P815B cells at $1x10^6$ in 5 mL (6-well plate) were incubated in DMEM (1% DMSO) with the desired compound concentration and for the appropriate amount of time (3, 6 or 24h). Following incubation, the cells were treated and stained following the protocol of FITC Annexin V Apoptosis Detection Kit with PI (BioLegend, USA). Analysis by flow cytometry was performed on a BD FACSVerse Flow Cytometer (BD Bioscience, USA). Data obtained from the equipment were analyzed using the FlowJo software.

4.11. Cell cycle assay

To synchronize the cells prior to the experiment, P815B cells were serum deprived for 24 h, before being resupplied with fresh DMEM containing 10 % of FBS. Then, tested compound in DMSO (final

concentration 1%) was added, and the cells were incubated for the appropriate time. Following incubation, $5x10^5$ cells were harvested and centrifuged 5 min. at 300 RCF. The pellet was washed twice with 200 μL of PBS and then resuspended in 200 μL of PBS. Next, while gently vortexing, 800 μL of a cold aqueous solution containing 70 % of ethanol were added to fix the cells that were stored at -20 °C. Right before the analysis, cells were washed twice with 5 mL of PBS and centrifuged 5 min. at 300 RCF. Finally, 200 µL of PBS containing 70 µg/mL of PI were added to the pellet and the sample was analyzed by flow cytometry.

4.12. ROS Measurement

To investigate whether the compounds caused an oxidative stress in P815B cells, production of H_2O_2 was evaluated using the bioluminescent ROS-Glo™ H_2O_2 Assay (Promega Inc., USA) according to the manufacturer's protocol. P815B cells were seeded at 30.000 cells/well in 80 µL IMDM (1 % DMSO). Cells were incubated for 3 and 6h with the desired test compound. TBHP 50 µM was used as positive control and 1% DMSO was used as negative control. Cell-free controls of these conditions were performed to confirm that the evaluated compounds did not generate ROS without the cells. Relative Luminescence Units (RLUs) were recorded on a GloMax spectrophotometer.

4.13. Microsomal stability

Liver microsomes (20 mg protein/ml), NADPH regenerating system solutions A & B and 10 mM stock compound solution (100% DMSO) were prepared. The reaction mixture finally contains 713 µL purified water, 200 µL 0.5 M potassium phosphate pH 7.4, 50 µL NADPH regenerating system solution A (BD Biosciences Cat. No. 451220), 10 µL NADPH regenerating system solution B (BD Biosciences Cat. No. 451200) and 2 µL of the compound stock solution (10 µM final concentration). A control experiment was realized for each compound by substituting NADPH regenerating solutions A and B for 60 µl of purified water. The reaction mixture is warmed to 37°C for 5 minutes in a water bath, and the reaction is initiated by the addition of 25 µL of liver microsomes (0.5 mg protein/ml final concentration). At different time points (0 min –60 min –180 min – 360 min – 24h), 100 µL is withdrawn and added to

400 µL cold acetonitrile on ice. Then the mixtures are centrifuged at 13 000 rpm for 5 min at 4°C. Finally, 450µl of the supernatant is recovered, evaporated using speedvac and evaluated by UPLC. Etoxycoumarine was used as a positive control.

4.14. Molecular Modelling

Molecular docking jobs were performed with AutodockVina 1.1.2,[50] using the disclosed tryptophan 2,3-dioxygenase structure (PDB ID: 5TI9)[38] with the orthosteric binding site occupied by natural ligand tryptophan, heme, and dioxygen. This structure was chosen as it displayed the full 338-346 loop that is part of this binding site. Hydrogens and charges were added then tryptophan and dioxygen were removed, centering the searching box 15 Å around this region. . Binding poses were analyzed for their binding mode and assessed in comparison with crystallized analog and with L-Trp.

4.15. LogK_w measurements

Samples were diluted in HPLC grade methanol at 0.1mg/mL then filtered with MILLEX-HV 0.45 µm, 4 mm (Millipore). The stationary phase was a C18 type column (Macherey-Nagel Nucleosil) with octadecyl grafting (5 µm, 15 cm x 4.6 mm). Mobile phases were a mixture of methanol and water stabilized at pH 2.3 with phosphoric acid in different proportions (90/10, 85/15, 80/20, 70/30, 60/40, 50/50, 40/60). All the mixtures were filtered with membrane filters PORAFIL 0.45 µm (Macherey-Nagel) prior used. Isocratic mode with a flow of 1mL/min was used and UV detection was performed at 238 nm. The HPLC has a pump in isocratic mode with a flow rate of 1mL/min. 20 µL of sample were manually injected three times in the loop of a Rheodyne injector.

Conflict of interest

The authors declare no conflict of interest.

Acknowledgements

This work is supported by Belgian *Fonds National de la Recherche Scientifique* (F.R.S.-FNRS; Grants 3.05557.43, 28252254 and 32704190), the Belgian *Fondation contre le Cancer* (Large Equipment grant), the French Community of Belgium (ARC 14/19- 058), the *Fonds Spéciaux de recherche* (FSR) at UCLouvain, and a J. Maisin Foundation grant. Arina Kozlova was PhD Fellow of the F.R.S.-FNRS.

The authors thank Esra Yildiz, Bénédicte Tollet, Marie-France Herent and Maude Bourlet for their technical support.

Appendix A. Supplementary data

Supplementary data to this article can be found online at

References

(1) Brown, N. Bioisosteres in Medicinal Chemistry. *Bioisosteres Med. Chem.* **2012**, *54*, 1–237.

(2) May, S. W. Selenium-Based Drug Design. *Top. Med. Chem.* **2016**, *17*, 87–118.

(3) Wessjohann, L. A.; Schneider, A.; Abbas, M.; Brandt, W. Selenium in Chemistry and Biochemistry in Comparison to Sulfur. *Biol. Chem.* **2007**, *388* (10), 997–1006.

(4) Moroder, L. Isosteric Replacement of Sulfur with Other Chalcogens in Peptides and Proteins. *J. Pept. Sci.* **2005**, *11* (4), 187–214.

(5) Mishra, K. K.; Singh, S. K.; Ghosh, P.; Ghosh, D.; Das, A. The Nature of Selenium Hydrogen Bonding: Gas Phase Spectroscopy and Quantum Chemistry Calculations. *Phys. Chem. Chem. Phys.* **2017**, *19* (35), 24179–24187.

(6) Howard, D. L.; Kjaergaard, H. G. Hydrogen Bonding to Divalent Sulfur. *Phys. Chem. Chem. Phys.* **2008**, *10* (28), 4113–4118.

(7) Jacob, C.; Giles, G. I.; Giles, N. M.; Sies, H. Sulfur and Selenium: The Role of Oxidation State in Protein Structure and Function. *Angew. Chemie Int. Ed.* **2003**, *42* (39), 4742–4758.

(8) Slater, J. C. Atomic Radii in Crystals. *J. Chem. Phys.* **1964**, *41* (10), 3199–3204.

(9) Batsanov, S. S. Van Der Waals Radii of Elements. *Inorg. Mater.* **2001**, *37* (9), 871–885.

(10) Brown, K.; Arthur, J. Selenium, Selenoproteins and Human Health: A Review. *Public Health Nutr.* **2001**, *4* (2b), 593–599.

(11) Holben, D. H.; Smith, A. M. The Diverse Role of Selenium within Selenoproteins: A Review. *J. Am. Diet. Assoc.* **1999**, *99* (7), 836–843.

(12) Bellinger, F. P.; Raman, A. V.; Reeves, M. A.; Berry, M. J. Regulation and Function of Selenoproteins in Human Disease. *Biochem. J.* **2009**, *422* (1), 11–22.

(13) May, S. W. Selenium-Based Pharmacological Agents: An Update. *Expert Opin. Investig. Drugs* **2002**, *11* (9), 1261–1269.

(14) Klein, E. A.; Thompson, I. M.; Tangen, C. M.; Crowley, J. J.; Lucia, S.; Goodman, P. J.; Minasian, L. M.; Ford, L. G.; Parnes, H. L.; Gaziano, J. M.; Karp, D. D.; Lieber, M. M.; Walther, P. J.; Klotz, L.; Parsons, J. K.; Chin, J. L.; Darke, A. K.; Lippman, S. M.; Goodman, G. E.; Meyskens, F. L.; Baker, L. H. Vitamin E and the Risk of Prostate Cancer: The Selenium and Vitamin E Cancer Prevention Trial (SELECT). *JAMA - J. Am. Med. Assoc.* **2011**, *306* (14), 1549–1556.

(15) Ali, W.; Benedetti, R.; Handzlik, J.; Zwergel, C.; Battistelli, C. The Innovative Potential of Selenium-Containing Agents for Fighting Cancer and Viral Infections. *Drug Discovery Today*. Elsevier Current Trends January 1, 2021, pp 256–263.

(16) Müller, A.; Cadenas, E.; Graf, P.; Sies, H. A Novel Biologically Active Seleno-Organic Compound-1. Glutathione Peroxidase-like Activity in Vitro and Antioxidant Capacity of PZ 51 (Ebselen). *Biochem. Pharmacol.* **1984**, *33* (20), 3235–3239.

(17) Singh, N.; Halliday, A. C.; Thomas, J. M.; Kuznetsova, O.; Baldwin, R.; Woon, E. C. Y.; Aley, P. K.; Antoniadou, I.; Sharp, T.; Vasudevan, S. R.; Churchill, G. C. A Safe Lithium Mimetic for Bipolar

Disorder. *Nat. Commun.* **2013**, *4* (1), 1–7.

(18) Masaki, C.; Sharpley, A. L.; Cooper, C. M.; Godlewska, B. R.; Singh, N.; Vasudevan, S. R.; Harmer, C. J.; Churchill, G. C.; Sharp, T.; Rogers, R. D.; Cowen, P. J. Effects of the Potential Lithium-Mimetic, Ebselen, on Impulsivity and Emotional Processing. *Psychopharmacology (Berl).* **2016**, *233* (14), 2655–2661.

(19) Parnham, M. J.; Sies, H. The Early Research and Development of Ebselen. *Biochem. Pharmacol.* **2013**, *86* (9), 1248–1253.

(20) Menéndez, C. A.; Byléhn, F.; Perez-Lemus, G. R.; Alvarado, W.; De Pablo, J. J. Molecular Characterization of Ebselen Binding Activity to SARS-CoV-2 Main Protease. *Sci. Adv* **2020**, *6*, 345–356.

(21) Jin, Z.; Du, X.; Xu, Y.; Deng, Y.; Liu, M.; Zhao, Y.; Zhang, B.; Li, X.; Zhang, L.; Peng, C.; Duan, Y.; Yu, J.; Wang, L.; Yang, K.; Liu, F.; Jiang, R.; Yang, X.; You, T.; Liu, X.; Yang, X.; Bai, F.; Liu, H.; Liu, X.; Guddat, L. W.; Xu, W.; Xiao, G.; Qin, C.; Shi, Z.; Jiang, H.; Rao, Z.; Yang, H. Structure of Mpro from SARS-CoV-2 and Discovery of Its Inhibitors. *Nature* **2020**, *582* (7811), 289–293.

(22) Wang, L.; Yang, Z.; Fu, J.; Yin, H.; Xiong, K.; Tan, Q.; Jin, H.; Li, J.; Wang, T.; Tang, W.; Yin, J.; Cai, G.; Liu, M.; Kehr, S.; Becker, K.; Zeng, H. Ethaselen: A Potent Mammalian Thioredoxin Reductase 1 Inhibitor and Novel Organoselenium Anticancer Agent. *Free Radic. Biol. Med.* **2012**, *52* (5), 898–908.

(23) Tombline, G.; Donnelly, D. J.; Holt, J. J.; You, Y.; Ye, M.; Gannon, M. K.; Nygren, C. L.; Detty, M. R. Stimulation of P-Glycoprotein ATPase by Analogues of Tetramethylrosamine: Coupling of Drug Binding at the “R” Site to the ATP Hydrolysis Transition State. *Biochemistry* **2006**, *45* (26), 8034–8047.

(24) Wiles, J. A.; Phadke, A. S.; Bradbury, B. J.; Pucci, M. J.; Thanassi, J. A.; Deshpande, M. Selenophene-Containing Inhibitors of Type IIA Bacterial Topoisomerases. *J. Med. Chem.* **2011**,

54 (9), 3418–3425.

(25) Plano, D.; Karelia, D. N.; Pandey, M. K.; Spallholz, J. E.; Amin, S.; Sharma, A. K. Design, Synthesis, and Biological Evaluation of Novel Selenium (Se-NSAID) Molecules as Anticancer Agents. *J. Med. Chem.* **2016**, *59* (5), 1946–1959.

(26) Ghiazza, A. C.; Billard, T.; Dickson, C.; Tlili, A.; Gampe, C. Chalcogen OCF3-Isosteres Modulate Drug Properties without Introducing Inherent Liabilities. *ChemMedChem* **2019**, *14* (17), 1586–1589.

(27) Zhao, L.; Zhao, G.; Xue, Q. Tizanidine (Hydrochloride) Inhibits A549 Lung Cancer Cell Proliferation and Motility through Regulating Nischarin. *Onco. Targets. Ther.* **2020**, *13*, 291–298.

(28) Xing, X. W.; Sun, Y. F.; Zhao, J.; Pan, Z. X.; Jiang, W. X. Tizanidine Hydrochloride Exhibits a Cytotoxic Effect on Osteosarcoma Cells through the PI3K/AKT Signaling Pathway. *J. Int. Med. Res.* **2019**, *47* (8), 3792–3802.

(29) Plano, D.; Moreno, E.; Font, M.; Encío, I.; Palop, J. A.; Sanmartín, C. Synthesis and in Vitro Anticancer Activities of Some Selenadiazole Derivatives. *Arch. Pharm. (Weinheim).* **2010**, *343* (11–12), 680–691.

(30) Ruberte, A. C.; Plano, D.; Encío, I.; Aydillo, C.; Sharma, A. K.; Sanmartín, C. Novel Selenadiazole Derivatives as Selective Antitumor and Radical Scavenging Agents. *Eur. J. Med. Chem.* **2018**.

(31) Pilotte, L.; Larrieu, P.; Stroobant, V.; Colau, D.; Dolusic, E.; Frederick, R.; De Plaen, E.; Uyttenhove, C.; Wouters, J.; Masereel, B.; Van den Eynde, B. J. Reversal of Tumoral Immune Resistance by Inhibition of Tryptophan 2,3-Dioxygenase. *Proc. Natl. Acad. Sci.* **2012**, *109* (7), 2497–2502.

(32) Hoffmann, D.; Dvorakova, T.; Stroobant, V.; Bouzin, C.; Daumerie, A.; Solvay, M.; Klaessens, S.; Letellier, M. C.; Renauld, J. C.; van Baren, N.; Lelotte, J.; Marbaix, E.; van den Eynde, B. J.

Tryptophan 2,3-Dioxygenase Expression Identified in Human Hepatocellular Carcinoma Cells and in Intratumoral Pericytes of Most Cancers. *Cancer Immunol. Res.* **2020**, *8* (1), 19–31.

(33) Terai, M.; Londin, E.; Rochani, A.; Link, E.; Lam, B.; Kaushal, G.; Bhushan, A.; Orloff, M.; Sato, T. Expression of Tryptophan 2,3-Dioxygenase in Metastatic Uveal Melanoma. *Cancers (Basel).* **2020**, *12* (2), 405.

(34) Fallarino, F.; Grohmann, U.; You, S.; McGrath, B. C.; Cavener, D. R.; Vacca, C.; Orabona, C.; Bianchi, R.; Belladonna, M. L.; Volpi, C.; Santamaria, P.; Fioretti, M. C.; Puccetti, P. The Combined Effects of Tryptophan Starvation and Tryptophan Catabolites Down-Regulate T Cell Receptor ζ-Chain and Induce a Regulatory Phenotype in Naive T Cells. *J. Immunol.* **2006**, *176* (11), 6752–6761.

(35) Mezrich, J. D.; Fechner, J. H.; Zhang, X.; Johnson, B. P.; Burlingham, W. J.; Bradfield, C. A. An Interaction between Kynurenine and the Aryl Hydrocarbon Receptor Can Generate Regulatory T Cells. *J. Immunol.* **2010**, *185* (6), 3190–3198.

(36) Routy, J. P.; Routy, B.; Graziani, G. M.; Mehraj, V. The Kynurenine Pathway Is a Double-Edged Sword in Immune-Privileged Sites and in Cancer: Implications for Immunotherapy. *Int. J. Tryptophan Res.* **2016**, *9* (1), 67–77.

(37) Kozlova, A.; Thabault, L.; Liberelle, M.; Klaessens, S.; Prévost, J. R. C.; Mathieu, C.; Pilotte, L.; Stroobant, V.; Van den Eynde, B.; Frédérick, R. Rational Design of Original Fused-Cycle Selective Inhibitors of Tryptophan 2,3-Dioxygenase. *J. Med. Chem.* **2021**, DOI: 10.1021/acs.jmedchem.1c00323.

(38) Lewis-Ballester, A.; Forouhar, F.; Kim, S. M.; Lew, S.; Wang, Y.; Karkashon, S.; Seetharaman, J.; Batabyal, D.; Chiang, B. Y.; Hussain, M.; Correia, M. A.; Yeh, S. R.; Tong, L. Molecular Basis for Catalysis and Substrate-Mediated Cellular Stabilization of Human Tryptophan 2,3-Dioxygenase. *Sci. Rep.* **2016**, *6* (35169).

(39) Thakur, A.; Zhang, K.; Louie, J. Suzuki-Miyaura Coupling of Heteroaryl Boronic Acids and Vinyl Chlorides. *Chem. Commun.* **2012**, *48* (2), 203–205.

(40) Knapp, D. M.; Gillis, E. P.; Burke, M. D. A General Solution for Unstable Boronic Acids: Slow-Release Cross-Coupling from Air-Stable MIDA Boronates. *J. Am. Chem. Soc.* **2009**, *131* (20), 6961–6963.

(41) Pham, K. N.; Lewis-Ballester, A.; Yeh, S. R. Conformational Plasticity in Human Heme-Based Dioxygenases. *J. Am. Chem. Soc.* **2021**, *143* (4), 1836–1845.

(42) Terentis, A. C.; Freewan, M.; Sempértegui Plaza, T. S.; Raftery, M. J.; Stocker, R.; Thomas, S. R. The Selenazal Drug Ebselen Potently Inhibits Indoleamine 2,3-Dioxygenase by Targeting Enzyme Cysteine Residues. *Biochemistry* **2010**, *49* (3), 591–600.

(43) Röhrig, U. F.; Majjigapu, S. R.; Vogel, P.; Zoete, V.; Michielin, O. Challenges in the Discovery of Indoleamine 2,3-Dioxygenase 1 (IDO1) Inhibitors. *J. Med. Chem.* **2015**, *58* (24), 9421–9437.

(44) Tsopelas, F.; Tsantili-Kakoulidou, A.; Ochsenkühn-Petropoulou, M. Investigation of the Chromatographic Behaviour of Some Selenium Species-Comparison with Their Octanol-Water Partitioning. *Talanta* **2007**, *73* (1), 127–133.

(45) Ayouni, L.; Cazorla, G.; Chaillou, D.; Herbreteau, B.; Rudaz, S.; Lantéri, P.; Carrupt, P. A. Fast Determination of Lipophilicity by HPLC. *Chromatographia* **2005**, *62* (5–6), 251–255.

(46) Elmansi, H.; Nasr, J. J.; Rageh, A. H.; El-Awady, M. I.; Hassan, G. S.; Abdel-Aziz, H. A.; Belal, F. Assessment of Lipophilicity of Newly Synthesized Celecoxib Analogues Using Reversed-Phase HPLC. *BMC Chem.* **2019**, *13* (1), 84.

(47) ACD/Percepta, 14.1.0 (Build 2921), Advanced Chemistry Development, Inc., Toronto, On, Canada, Www.Acdlabs.Com, 2021.

(48) Swain, M. Chemicalize.Org. *J. Chem. Inf. Model.* **2012**, *52* (2), 613–615.

(49) Schiemann, K.; Stieber, F.; Esdar, C. Azaheterocyclic Compounds. WO/2014/086453, 2014.

(50) Oleg Trott; Arthur J. Olson. AutoDock Vina: Improving the Speed and Accuracy of Docking with a New Scoring Function, Efficient Optimization, and Multithreading. *J. Comput. Chem.* **2010**, *31* (2), 455–461.